Phase-space single electron-hole acceleration

Physics of Plasmas

RESEARCH ARTICLE | FEBRUARY 24 2025

Phase-space single electron-hole acceleration

A. Guillevic ; M. Lesur ; D. Mandal ; X. Garbet ; E. Gravier ; G. Lo-Cascio ; A. Ghizzo ; T. Réveillé

Phys. Plasmas 32, 022117 (2025)
https://doi.org/10.1063/5.0246056

Physics of Plasmas ARTICLE pubs.aip.org/aip/pop

Phase-space single electron-hole acceleration

Cite as: Phys. Plasmas **32**, 022117 (2025); doi: 10.1063/5.0246056
Submitted: 30 October 2024 · Accepted: 10 February 2025 ·
Published Online: 24 February 2025

A. Guillevic,[1,2,a] M. Lesur,[1] D. Mandal,[1,3] X. Garbet,[4,5] E. Gravier,[1] G. Lo-Cascio,[1] A. Ghizzo,[1] and T. Réveillé[1]

AFFILIATIONS

[1]Université de Lorraine, CNRS – IJL, F-54000 Nancy, France
[2]Chalmers University of Technology, 412 96 Gothenburg, Sweden
[3]Techno India University, Sector-V, Bidhannagar, Kolkata 700091, India
[4]CEA, IRFM, F-13108 Saint-Paul-lez-Durance, France
[5]School of Physical and Mathematical Sciences, Nanyang Technological University, 637371 Singapore

[a)]Author to whom any correspondence should be addressed: alejandro.guillevic@chalmers.se

ABSTRACT

Single electron-hole dynamics in a one-dimensional plasma composed of two species, electrons and protons, with reduced mass ratio, is investigated through numerical kinetic Vlasov–Maxwell simulations. The electron-hole's growth of phasetrophy and acceleration are systematically studied as a function of different plasma and electron-hole parameters such as electron drift velocity v_d, initial hole velocity δv_h, electric potential amplitude ϕ_0, and gradients of the distribution functions $f'_{e,h}$ and $f'_{i,h}$. A first parameter scan shows two different regimes of positive exponential increase for the electron-holes growth-rate at both positive and negative gradient sides of the electron distribution function. Linear growth of an electron-hole is observed as a function of both ion and electron distribution functions. Moreover, two power laws are measured as a function of the electric potential amplitude in both low- and high-amplitude regimes. Finally, a qualitative agreement between measurements of phasetrophy growth-rate against an effective gradient is found, the latter considering variations and effects of the electron distribution function gradient over the electron-hole's width.

I. INTRODUCTION

The dynamics of electron-holes in plasmas have long been recognized as a fundamental area of research in plasma physics due to their critical role in plasma turbulence and transport and the subsequent impact on energy distribution and stability within both natural and laboratory plasmas. Electron-holes are typically characterized as localized negative phase-space density perturbation of the electron distribution function, which emerge as self-consistent phase-space structures that propagate and explore large regions of the plasma while remaining stable over time. These structures are of particular interest due to their nonlinear interactions with the plasma, which can lead to complex dynamical behaviors, including acceleration and deceleration, growth in size and depth, the sub-critical triggering of plasma instabilities,[1] and the interaction between different structures in both experiments[2,3] and numerical simulations.[4–6] Indeed, phase-space structures can drive particle transport,[7,8] modify the saturation amplitude,[9] drive anomalous resistivity,[10] shift the mode frequency,[7] yield amplitude oscillations or chaos,[11] and couple with zonal flows.[12]

The analysis of electron-hole dynamics is not merely of theoretical interest but is critical for understanding a wide range of phenomena, such as those in space and astrophysical plasmas,[13,14] or those observed in the Earth's magnetosphere[15–17] or magnetic reconnection events[18,19] where collisionless plasmas prevail. For laboratory plasmas, electron-holes are relevant in the context of energetic particle-driven activities such as in magnetically confined fusion devices,[20] collisionless shock waves,[21] and drift-waves,[22] which can influence particle transport, energy dissipation, and confinement stability. Despite their significance, many aspects of electron-hole behavior, such as their growth, acceleration, and the quantitative effects on plasma turbulence, remain poorly understood.

An electron-hole's stability in phase-space is a delicate balance between the electromagnetic forces of the plasma and the momentum associated with the hole. In the second half of the *XXth* century, observation in a variety of stellar,[16] laboratory,[23] and numerical plasmas[6,24,25] proved the existence of electron-holes rich dynamics, including acceleration, growth, decay, and binary interactions. In the early 80s, analytical[26–29] and numerical[30,31] papers proposed a theory

predicting the acceleration and growth-rate of phase-space holes. However, limitations on computational tools constrained their ability to capture the nonlinear and multi-dimensional aspects of the problem in its entirety. It is not until the past few decades, through the improvements in diagnostics in spacecraft[17] for data collection. In computing power, which enabled more precise and detailed studies through the use of high-resolution numerical simulations.[32–37] This allows for a more comprehensive exploration of electron-hole dynamics across a broader range of parameters.

This study seeks to build upon this body of knowledge by conducting a high-definition numerical investigation of single electron-hole dynamics by means of the kinetic Vlasov–Maxwell code COBBLES (COnservative Berk-Breizman semi-Lagrangian Extended Solver).[38,39] This research aims to identify the key parameters influencing electron-hole acceleration and growth by systematically varying the initial conditions, shape, and plasma parameters, such as electron drift velocity, initial hole velocity, electric potential, size, depth, and gradients of the distribution functions. These simulations offer new insights into the underlying mechanisms that drive electron-hole growth, acceleration, and interactions.

In Sec. II, the Vlasov–Maxwell model and Schamel electron-hole distribution functions[40] are presented. We introduce the electron-hole growth and acceleration mechanism and time plots, in the case of a single electron-hole, in Sec. III. Numerical results, as a function of plasma and electron-hole parameters, are reported in Sec. IV. Finally, a conclusion is provided in Sec. V.

II. MODEL

A. Model description

Our model describes the evolution of a two-species, 1D1V (one spatial dimension and one velocity dimension), collisionless, electrostatic plasma. A 1D1V plasma model is not only relevant as an academic exercise but essential for describing various processes in more complex dimensions, such as for a plasma in a strong, homogeneous magnetic field,[41] or to model energetic particle transport on Tokamaks.[42] Here, the evolution of the species s particle distribution function $f_s(x, v, t)$, where $s = i, e$ for hydrogen ions and electrons, is given by the Vlasov equation:

$$\frac{\partial f_s}{\partial t} + v\frac{\partial f_s}{\partial x} + \frac{q_s}{m_s}E(x,t)\frac{\partial f_s}{\partial v} = 0, \tag{1}$$

where $E(x, t)$ is the electric field, and q_s and m_s are the particle charge and mass, respectively.

On the other hand, the evolution of the electric field E satisfies the Maxwell-current equation:

$$\frac{\partial E}{\partial t} = -\sum_s \frac{m_s\omega_{P,s}^2}{n_0 q_s}\int_{-\infty}^{+\infty} v f_s(x, v, t)dv, \tag{2}$$

where $\omega_{P,s}$ is the plasma frequency of species s and n_0 is the spatially averaged plasma density. Here the initial electric field is obtained by solving Poisson's equation:

$$\frac{\partial E}{\partial x} = \sum_s \frac{q_s}{\varepsilon_0}\int_{-\infty}^{+\infty} f_s(x, v, t)dv, \tag{3}$$

where ε_0 is the vacuum permittivity constant. We define the quantity $\delta f_s \equiv f_s - \langle f_s\rangle$, where $\langle f_s\rangle = \langle f_s\rangle(v, t)$ is the spatially averaged distribution function in a box of length L. Note that in this study, we impose the quasi-neutrality condition in the box, which for a hydrogen plasma ($q_i = e$) reduces to

$$\int_0^L\int_{-\infty}^{+\infty} f_i(x, v, t)dvdx - \int_0^L\int_{-\infty}^{+\infty} f_e(x, v, t)dvdx = 0. \tag{4}$$

Numerically, we simulate the two-species plasma employing the self-consistent kinetic electrostatic code COBBLES.[38,39] COBBLES solves the one-dimensional kinetic Vlasov–Maxwell system using a semi-Lagrangian method[43] through a Cubic-Interpolated-Propagation scheme. One property of COBBLES is that it exactly conserves elements of phase-space.[44]

Hereafter, we impose the physical parameters of our plasma. The mass ratio $m_i/m_e = 36$ is chosen to reduce the total simulation time, as it allows for a less defined phase-space grid, which also improves the readability of the distribution functions in phase-space. Both ion and electron temperatures are equal $T_i = T_e$, whereas the simulation box size $L = 2\pi/k$, where $k = 0.2\lambda_D^{-1}$ is the first mode wave number. The equilibrium velocity distribution function for each species is a Gaussian,

$$f_{s,0}(v) = \frac{n_{s,0}}{v_{s,T}\sqrt{2\pi}}\exp\left[-\frac{1}{2}\left(\frac{v - v_{s,0}}{v_{s,T}}\right)^2\right], \tag{5}$$

where $n_{s,0}$ is the initial particle density, $v_{s,T}$ is the thermal velocity, and $v_{s,0}$ is the initial mean velocity of the distribution functions with $v_{i,0} = 0$ and $v_{e,0} = v_d \leq v_{e,T}$. Note that in this paper, the system is in the stable regime since we chose the mean velocities to be below the critical unstable mean velocity difference of $v_{cr} \simeq 1.5v_{e,T}$. Boundary conditions are periodic in the real space, while in the velocity space, we ensure zero particle flux at the velocity cutoffs $v_{e,cut} = [-6v_{e,T}; +6v_{e,T}]$ and $v_{i,cut} = [-6v_{i,T}; +18v_{i,T}]$. All simulations are performed with $N_x = 4096$ and $N_v = 4096$ grid points in real and velocity space, respectively, while the time step is fixed at $\Delta t = 0.01\omega_P^{-1}$. Note that all physical quantities are normalized to the electron characteristic quantities, namely, the electron thermal velocity $v_T = v_{e,T}$, electron Debye length $\lambda_D = \lambda_{e,D}$, electron plasma oscillation $\omega_P = \omega_{e,P}$, and initial particle density $n_0 = n_{i,0} = n_{e,0}$.

B. Generalized electron-holes

Particle distributions often deviate from Gaussian distributions in high-temperature collisionless plasmas, such as fusion, ionospheric, or astrophysical plasmas. Multiple studies, analytical,[27,40,45] numerical,[46,47] and experimental,[47] have shown the existence of self-consistent steady-state nonlinear solutions to the Vlasov–Poisson system of equations known as BGK (Bernstein–Green–Kruskal) structures/modes.[45] These solutions represent nonlinear electrostatic waves that propagate and trap plasma particles. These trapped particles play an essential role in the transport of particles and energy, instability triggering, and disturbance on plasma confinement.

The BGK method, or the integral approach method, aims to derive a trapped particle distribution function given an, often physical, electric potential $\phi(x)$, and distribution of free particles. The downside of such a method is that the resulting distribution function of trapped particles may not be stable over time or physically meaningful, often resulting in distribution functions with negative values or singularities.

A differential approach, also known as a pseudo-potential, Sagdeev, or Schamel method, is used to overcome the problems associated with the BGK method. This approach proceeds in the opposite manner; it imposes a physically meaningful distribution function, from which a self-consistent electric potential is obtained by solving the corresponding Vlasov–Poisson system.

One distribution function known to satisfy the continuity and positivity condition and produce a phase-space structure is the Schamel distribution function,[40,48,49]

$$f_{s,h}(x,v) = \frac{n_{s,0}}{v_{s,T}\sqrt{2\pi}} = \exp\left[-\frac{1}{2}\left(\frac{\delta v_{s,h}}{v_{s,T}}\right)^2 - \beta_h \frac{E_s}{m_s v_{s,T}^2}\right] \quad (6)$$

if $E_s \leq 0$ and

$$f_{s,h}(x,v) = \frac{n_{s,0}}{v_{s,T}\sqrt{2\pi}} = \exp\left[-\frac{1}{2v_{s,T}^2}\left(\sigma_v\sqrt{2\frac{E_s}{m_s}} - \delta v_{s,h}\right)^2\right] \quad (7)$$

if $E_s > 0$, where $\delta v_{s,h} = v_{s,0} - v_{h,0}$ is the velocity shift between the mean velocity $v_{s,0}$ and the initial velocity $v_{h,0}$ of the BGK structure, $\sigma_v = \text{sign}(v - \delta v_{s,h})$ is the sign of the velocities difference. β_h is the trapping parameter, which determines the curvature of the structure: $\beta_h < 0$ is a hole, $\beta_h = 0$ a plateau, and $\beta_h > 0$ for a bump in the distribution function. E_s is the particle energy of species s, defined by

$$E_s(x,v) = \frac{1}{2}m_s(v - (v_{s,0} - \delta v_{s,h}))^2 + q_s\phi(x - x_h), \quad (8)$$

where $\phi(x)$ is the Schamel electric potential of a structure centered at $x = x_h$. In this paper, we focus on the study of electron-holes, in other words, $\beta_h < 0$, which result from bell-shaped electric potentials of the form sech^4, of amplitude ϕ_0 at $x = x_h$, where the skirts converge to $\phi = 0$ in the limit $|x - x_h| \to +\infty$. The electron-hole potential is given by

$$\phi(x) = \phi_0\,\text{sech}^4\left(\frac{x - x_h}{\Delta x_h}\right), \quad (9)$$

where Δx_h is the structure characteristic width defined by the hole parameters:

$$\Delta x_h = \sqrt{\sqrt{\frac{\pi}{\phi_0}}\frac{15\exp\left(\delta v_{s,h}^2/2\right)}{(1 - \beta_h - \delta v_{s,h}^2)}}. \quad (10)$$

Figure 1 shows a slice of the electron equilibrium distribution function $f_{e,0}$ and Schamel distribution function $f_{e,h}$ for an electron-hole. Moreover, Fig. 2 shows the typical Schamel sech^4 electric potential for an electron-hole in phase-space from Eq. (9).

Note that to satisfy both the quasi-neutrality condition, i.e., Eq. (4), and equal initial particle density $n_{i,0} = n_{e,0}$, one of the three free electron-hole parameters, δv_h, ϕ_0, or β_h, must be constrained and be a function of the other two. In this study, we chose this parameter as the trapping parameter β_h. We developed a minimization algorithm that searches to optimize the Schamel sech^4 phase-space hole β_h parameter for quasi-neutrality in the simulation box.[37] This algorithm produces a single β_h value for every combination of hole and plasma parameters. One shortcoming of constraining the structure to a periodic simulation box is the inability to perform a parameter scan where only one hole parameter is modified since any variation on hole parameters results in a variation on β_h. Nevertheless, this study considers that changes in β_h have negligible effects on electron-hole dynamics compared to changes on other hole parameters like for δv_h or ϕ_0.

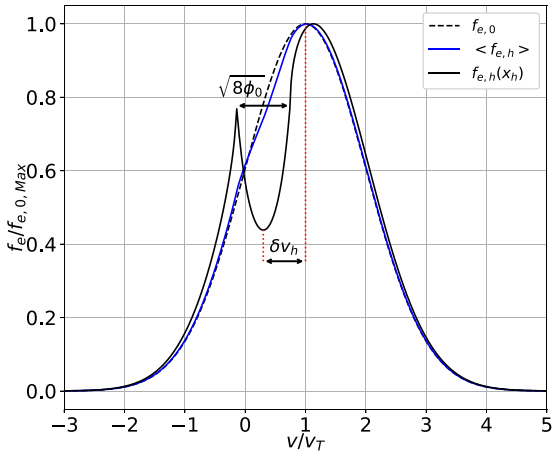

FIG. 1. Electron Schamel distribution function slice at $x = x_h$ normalized to the maximum of the electron equilibrium distribution function $f_{e,0,max} = n_{s,0}/v_{e,T}\sqrt{2\pi}$, for a mass ratio of $m_i/m_e = 36$, and parameters $\phi_0 = 0.10$, $\beta_h = -5.80$, and $\delta v_h = 0.70 v_T$.

III. SINGLE ELECTRON-HOLE DYNAMICS

A. Electron-hole's growth and acceleration

A phase-space structure exhibits complex phase-space dynamics, specifically, the growth and decay that result from an electron-hole climbing the gradients of the electron and ion distribution functions.

In a plasma, an electron-hole represents a region of plasma with a deficit of electrons, in other words, a region of phase-space with a local positive charge. In this case, one can consider an electron-hole as a quasiparticle with negative mass and positive charge.[6] Due to the electron-hole's local electric field, the electron distribution's free electrons are pulled toward the hole. This process results in an energy exchange that accelerates the trapped electrons to phase-space regions

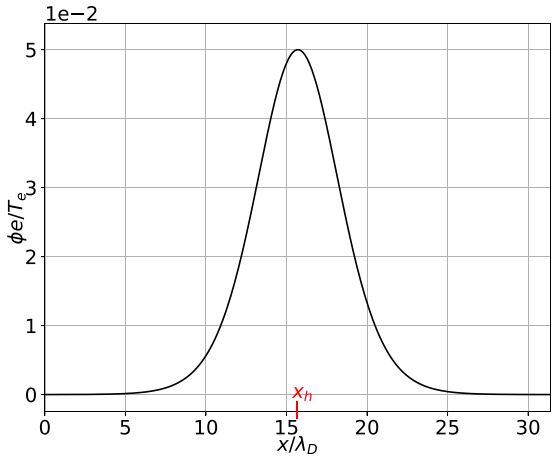

FIG. 2. Electron-hole Schamel sech^4 hole-potential with amplitude $\phi_0 = 0.05 T_e/e$.

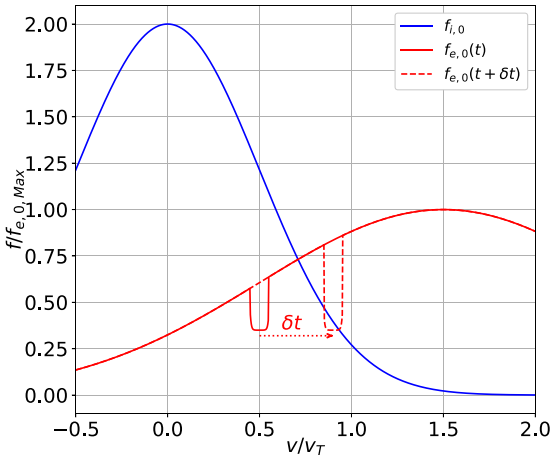

FIG. 3. Diagram of an electron-hole between the electron and ion distributions, growth, and acceleration mechanism after a δt time. Normalized equilibrium distribution functions: Ion in blue and electron in solid red. Normalized electron distribution, including the electron-hole in dashed red. The mass ratio and the drift velocity are decreased for the readability of the diagram, $m_i/m_e = 4$ and $v_d = 1.5v_T$, respectively.

with a larger distribution function value. Furthermore, as the hole accelerates, its depth increases since the distribution function value must remain constant along particle trajectories to satisfy Liouville's theorem. This process is depicted in Fig. 3, where a narrow-square electron-hole at low velocity grows in depth and accelerates to a higher velocity in a short time while climbing the electron distribution function.

Clumps, including electron-hole, generally tend to break apart due to particle collisions and electromagnetic turbulence in the plasma during their lifetime. However, if these collisional and electromagnetic effects occur over time scales much larger than the lifetime of an electron-hole (which is relevant for our studies and fusion plasmas), a clump can grow before decaying. This manuscript investigates the rate at which electron-holes grow before they start to decay.

To measure the electron-hole growth-rate, we measure the electron-hole's phasetrophy[50,51] ψ_h, which stands for phase-space enstrophy, which is a quantity equivalent to the enstrophy for a two-dimensional (2D) ideal fluid. Phase-space structures remarkably resemble 2D vortice fluid turbulence,[52] not just because of their shape but also because both systems are constrained by two invariants: wave energy and the phasetrophy (distribution perturbation square) for a Vlasov plasma and the energy and enstrophy (mean square vorticity) for fluids.

For a 1D1V plasma, phasetrophy is defined as

$$\psi_h = \int \langle \delta f_e^2 \rangle dv, \tag{11}$$

where $\langle \delta f^2 \rangle$ is the spatial average of the distribution perturbation squared. The phasetrophy growth-rate defined as

$$\gamma_h = \frac{1}{\psi_h}\frac{d\psi_h}{dt}. \tag{12}$$

By using the conservation of $\int f_e^2 dv$, substituting the derivative with the conservation of phase-space density, and performing integration by parts, the expression for the phasetrophy production is obtained as[37]

$$\gamma_h = -\frac{2}{\psi_h}\frac{q_e}{m_e}\int \frac{d\langle f_e \rangle}{dv}\langle E\delta f_e \rangle dv. \tag{13}$$

Assuming that in the velocity interval Δv_h bounded by the electron-hole velocity-width, the gradient of f_e remains constant, then $\frac{d\langle f_e \rangle}{dv}$ can be taken out of the integral. The remaining term, proportional to the electric field and the distribution perturbation $\frac{q_e}{m_e}\int \langle E\delta f_e \rangle dv$, is defined as the electron-hole acceleration,

$$\gamma_h = -\frac{2}{\psi_h}\frac{d\langle f_e \rangle}{dv}a_h. \tag{14}$$

This shows a dependency on the gradient of the electron distribution and the electric field (or potential). Previous studies and simulations[1,31,37] have shown a more complex dependency on the growth-rate of electron-holes than initially expected. As mentioned and depicted in Fig. 3, the growth-rate of a hole strongly depends on the ion and electron gradients and the shape of the hole. Subsequently, a hole with a more complex shape, such as a Schamel's hole or simply one with a larger width, will behave differently than a simple small square hole.

B. Time evolution of a single electron-hole

An electron-hole is considered to be in a growth regime when the hole's velocity is in the range[1,31,37] $0 < v_h < v_d$, which in terms of Schamel's parameters corresponds to $\delta v_h > 0$. Note that small values of δv_h mean an electron-hole located near the maxima of the electron distribution function. In contrast, a large $\delta v_h \sim v_d$ corresponds to an electron-hole close to the ion distribution function maxima.

As a benchmark, we performed the simulation of one electron-hole with parameters $v_d = 1v_T$, $\phi_0 = 0.05T_e/e$, $\beta_h = -6.56$, and $\delta v_h = 0.45v_T$. This corresponds to a relatively small electron-hole with a velocity-width of $\Delta v_h = 0.32v_T$. In Fig. 4, we show the time evolution of the electron-hole velocity, hole phasetrophy, and depth. Note that the depth of a hole, in terms of f, is a conserved quantity since the Vlasov equation states that the phase-space distribution function $f(x, v)$ along particle trajectories is conserved. Therefore, as the hole grows, δf_e must decrease.

In Fig. 4, we observe the expected tendency to increase for both the hole velocity and phasetrophy and verify that the value of the distribution at the center of the hole remains constant over time. In the velocity and phasetrophy, we observe three different regimes of growth. First, for times smaller than $100\omega_P^{-1}$, the velocity and phasetrophy amplitudes have a considerable nonlinear change. This is because, at these initial times, the analytical electron-hole's shape is modified self-consistently due to the interaction with the ion distribution, until it reaches a time-stable shape. Second, for times between $100\omega_P^{-1}$ and $400\omega_P^{-1}$, we observe a linear increase in the electron-hole's velocity and exponential growth of the phasetrophy, which corresponds to an acceleration of $1.49 \times 10^{-4}v_T\omega_P$ ($1.06 \times 10^{-3}v_T\omega_b$) and a growth-rate of $4.16 \times 10^{-4}\omega_P$ ($2.95 \times 10^{-3}\omega_b$), where ω_b is the bounce frequency of the deepest trajectories of the electron-hole defined as $\omega_b = \sqrt{k^2\phi_0/m_e}$. Third, after $400\omega_P^{-1}$, we observe a decrease in the amplitudes of both velocity and phasetrophy of the

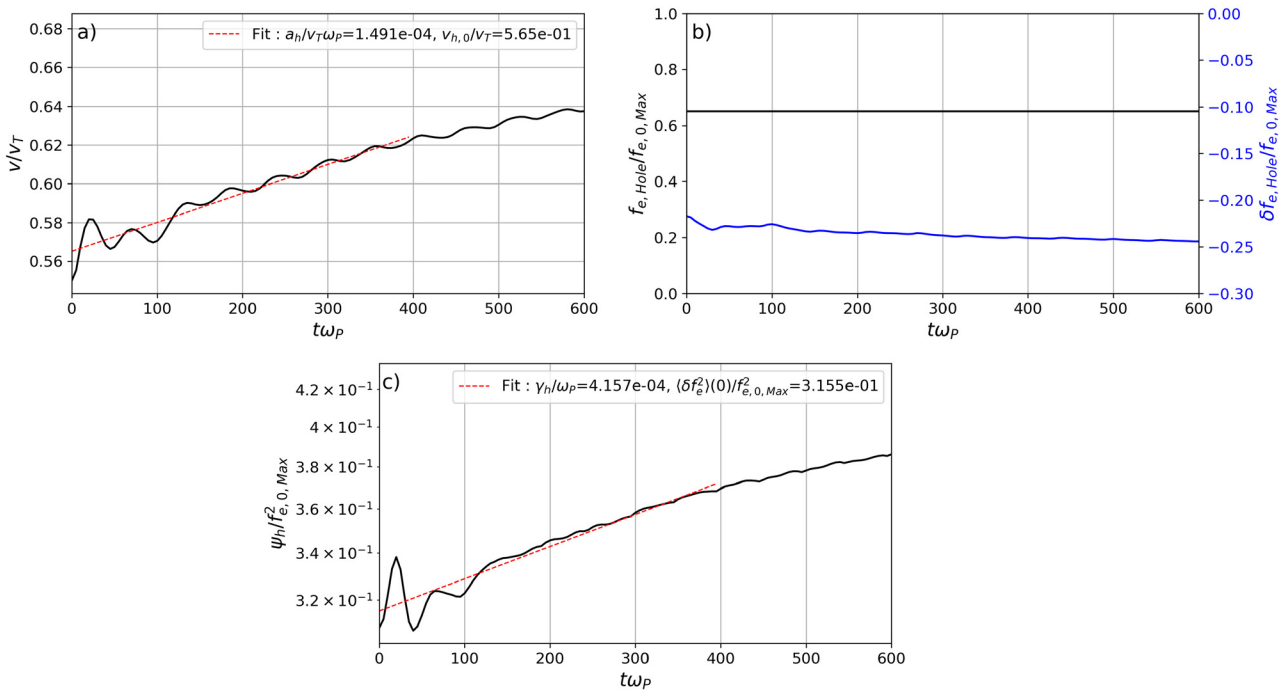

FIG. 4. Time evolution of an electron-hole. Initial parameters here correspond to the hole velocity in (a), values of f_e and δf_e hole depth in (b), and the hole phasetrophy in (c). For initial parameters: $v_d = 1v_T$, $\phi_0 = 0.05T_e/e$, $\beta_h = -6.56$, and $\delta v_h = 0.45v_T$.

electron-hole. This decrease in amplitude is mainly due to the hole accelerating and *climbing* the electron distribution function, resulting in different ion and electron gradients than at the start of the simulation. The effect of ion and electron gradients is studied in more detail in Secs. IV B and IV C, respectively. Note the oscillations in the three plots (which are more noticeable in the velocity plot time evolution). They result from small changes in the hole's velocity since, as it accelerates, the ions and electrons push and pull on the electron-hole to find a stable equilibrium, which is only reachable after very large times, due to collisions or its numerical equivalent. Nonetheless, these variations are averaged in the interval we measure and do not contribute to the long-term acceleration and growth of the hole.

Hereafter, we focus on studying the phasetrophy growth-rate, contrary to the acceleration, since both measure the effects on the dynamics of a phase-space electron-hole. In Sec. IV, we investigate the growth-rate of electron-holes as a function of v_h, $\partial_v f_{e,0}|_{v_h}$, $\partial_v f_{i,0}|_{v_h}$, and ϕ_0, the hole's velocity, equilibrium electron and ion gradients, and hole's amplitude.

IV. RESULTS AND DISCUSSION

In this section, we conducted four sets of electron-hole simulations via a parameter scan by means of the velocity variance, equilibrium electron and ion gradients, and electric potential amplitude, δv_h, $\partial_v f_{e,0}$, $\partial_v f_{i,0}$, ϕ_0, respectively. Measuring growth rates through these parameters allows us to study the hole's velocity effects while maintaining the distributions' mean velocities constant, study the effects of the proximity of the hole with the distribution functions, and measure the impact of the size of the hole on its growth. Note, in the rest of this paper, the equilibrium electron and ion gradients are written as $f'_{e,h}$ and $f'_{i,h}$ for simplicity.

A. Relative hole velocity δv_h

First, we performed ten electron-hole simulations with base parameters $v_d = 1v_T$ and $\phi_0 = 0.05T_e/e$, with δv_h in the range from $0.65v_T$ up to $-0.30v_T$. These include five simulations where δv_h is positive, corresponding to a positive electron gradient $f'_{e,h} > 0$, and five other simulations for a negative or zero δv_h, corresponding to a negative $f'_{e,h} < 0$. Note that the ion gradient $f'_{i,h} < 0$ remains negative.

The growth-rate of the phasetrophy is plotted in Fig. 5 for these ten simulations as a function of the average relative electron-hole velocity at the measurement time. Instead of choosing to plot the figure as a function of the initial relative electron-hole velocity, we chose to use the average relative electron-hole velocity at the moment of the measurement, since as shown in Fig. 4 and explained in Sec. III B electron-holes experience an initial nonlinear acceleration. For electron-holes with low initial velocity or large relative hole velocity, this results in a significant difference between the beginning of the simulation and the start of the linear regime. However, this paper does not investigate the initial acceleration of electron-holes. Therefore, for this and the following measurements, we chose the velocity in the middle of the interval where the growth-rate and acceleration are measured.

First, we observe a discrepancy between the growth-rate γ_h obtained through the measurements of the phasetrophy and those obtained through the measurement of the electron-hole linear acceleration [Eq. (14)] for values of δv_h close to zero. For electron holes at velocities close to the mean velocity of the electron distribution, the

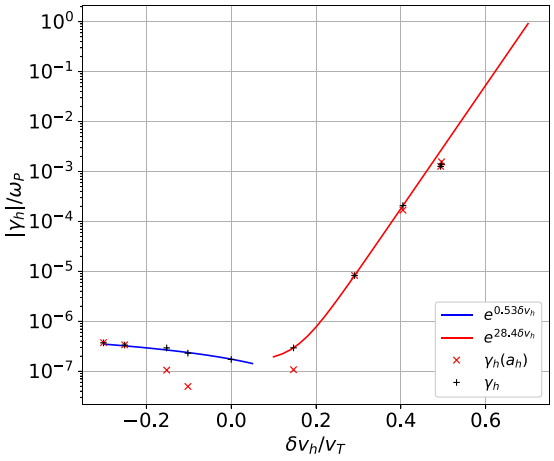

FIG. 5. Semi-log plot of the absolute value of the growth-rate of the electron-hole's phasetrophy as a function of the average relative electron-hole velocity at the moment of the measurement. The growth-rate from numerical simulations in black crosses, $\gamma_h(a_h)$ is the growth-rate calculated from the acceleration, and exponential fits of the growth-rate measurements in the two δv_h regimes in solid blue and red lines.

acceleration is analytically expected to be close to zero. Experimentally, it is difficult to properly measure the acceleration at such velocities since small variations in the plasma and structure shape itself can modify the measurement, which is not the case for the phasetrophy since it takes into account the plasma around the structure by integrating in both space and velocity as shown in Eq. (11). Nevertheless, for values of $|\delta v_h| > 0.2 v_T$, we observe quantitative and qualitative agreement between the two measurements of growth-rate. The correlation between the expected linear relationship of the growth-rate with the electron-hole's acceleration can be more directly observed in Fig. 6, where the growth-rate calculated from Eq. (14) deviate from the expected linear behavior for small values of the electron-hole's acceleration resulting from values of δv_h near zero.

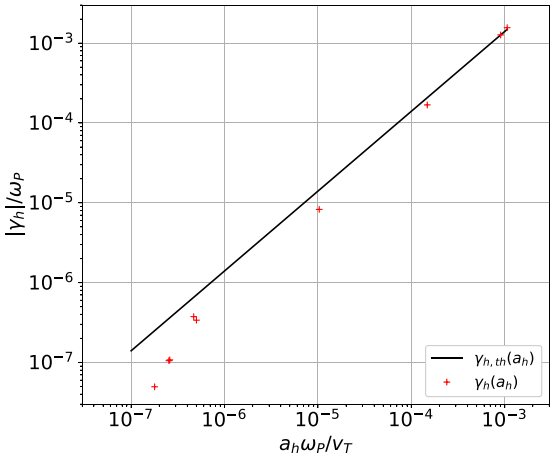

FIG. 6. Log-log plot of the absolute value of the growth-rate of the electron-hole's phasetrophy as a function of the electron-hole's acceleration. Black line: Analytical expression (14). Red crosses: measurements from numerical simulations.

Second, in Fig. 5, we observe two different growth regimes: a first one for positive δv_h, the growth-rate increases exponentially with the relative hole velocity. For zero or negative δv_h, we observe an exponential increase in the growth-rate with a decrease in δv_h. For values of δv_h between 0 and $0.45 v_T$, we measure an exponential fitting coefficient of $28.4/v_T$. For larger values of δv_h, we observe a discrepancy with respect to the exponential fitting, which we assume is the result of the electron-hole strongly interacting with the ion distribution function. Indeed, electron-holes with a hole velocity of the order of a few percent of the ion thermal velocity, $v_{T,i} \sim 0.17 v_T$, result in an increasingly important interaction between the hole and the ion distribution, which results in a strong and fast nonlinear initial acceleration, and growth-rate. Therefore, to measure a correct acceleration and growth-rate, we prefer to simulate electron-holes with a hole velocity superior to a few, three, or four ion thermal velocities to separate the electron-hole from the maximum of the ion distribution. For more details on the impacts of the ion distribution on electron-hole dynamics, see Sec. IV D, where the study of these effects is expanded.

In the case of zero or negative δv_h, between $-0.3 v_T$ and 0, we observe an exponential growth with a fitting coefficient of $-0.53/v_T$. Note that in this region, the phasetrophy decreases, and the hole decelerates. However, since it is challenging to show negative values on a logarithmic scale, we decided to show the absolute growth-rate instead. In this regime, the electron-hole experiences negative gradients for $f'_{i,h}$ and $f'_{e,h}$. While $f'_{i,h}$ remains relatively constant in this regime, $f'_{e,h}$ increases in amplitude with the decrease in δv_h, which results in a slight decrease in the electron-hole's phasetrophy, as opposed to the rapid increase with positive δv_h.

B. Local electron distribution gradient $\partial_v f_{e,0}$

We performed ten simulations at fixed electron-hole velocity at $v_h = 0.55 v_T$ and the amplitude of the Schamel potential at $\phi_0 = 0.05$ and varied the relative hole velocity in the interval $\delta v_h/v_T = [0.00, 0.60]$. This scan allows us to study the electron gradient $f'_{e,h}$ dependency on the phasetrophy growth-rate while

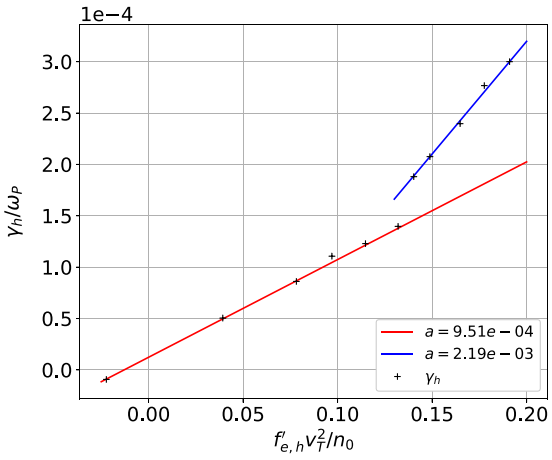

FIG. 7. Electron-hole phasetrophy growth-rate as a function of the electron equilibrium distribution gradient at the average hole velocity at the moment of the measurement. Growth-rate from numerical simulations in black crosses and linear fittings of the data in solid red and blue lines.

maintaining the ion gradient $f'_{i,h}$ constant between all the simulations. Note that in this scan, the electron mean velocity v_d is adjusted according to equation $v_d = \delta v_h - v_h$, assuming the values in the interval $v_d/v_T = [0.55, 1.15]$.

Figure 7 shows the phasetrophy growth-rate as a function of $f'_{e,h}$, at the average hole velocity at the measurement time. We observe a linear relationship between $f'_{e,h}$ and the phasetrophy growth-rate at small gradients, $f'_{e,h} < 15\%$, corresponding to values of $\delta v_h < 0.40 v_T$.

Additionally, we observe a second linear growth regime for values of the electron gradient larger than 14%, with a significantly steeper slope compared to for smaller values of the gradient. At these gradient values, the electron-hole is located at a phase velocity close to the ion distribution function maximum; in other words, the interaction between the electron-hole and the ion distribution becomes non-negligible. This results in a stronger nonlinear acceleration that is not present in the cases where the electron-hole is farther from the ion distribution maximum.

C. Local ion distribution gradient $\partial_v f_{i,0}$

We performed seven simulations at a fixed relative electron-hole velocity $\delta v_h = 0$ and Schamel potential amplitude $\phi_0 = 0.05$, while varying the hole velocity in the interval $v_h/v_T = [0.35, 1.00]$. The objective is to study the effects on the phasetrophy growth-rate due to changes in the ion gradient $f'_{i,h}$.

The growth-rate of the phasetrophy is plotted in Fig. 8 as a function of the absolute value of $f'_{i,h}$ at the average hole velocity at the measurement time. Similar to the results for $f'_{e,h}$, we observe a linear growth of the growth-rate with respect to $f'_{i,h}$. Note that Fig. 8 is in log-log scale, whereas the fitting is precisely linear. We observe an increase in the growth-rate with $f'_{i,h}$, which is to be expected since large values of $f'_{i,h}$ correspond to a hole located closer to the ion distribution (low hole velocity v_h). Note that we do not perform electron-hole simulations in the regime close to the ion distribution maxima, which would correspond to a small $f'_{i,h}$. Nevertheless, without requiring to perform simulations at such small hole velocities, we observe that electron-holes experience stronger effects of $f'_{i,h}$, in particular the effects related to the hole size in the velocity direction. In other words, these simulations experience similar effects to the "aberrant" points observed in Figs. 5 and 7.

On the other hand, for smaller values of $f'_{i,h}$, we observe that the phasetrophy growth-rate abruptly approaches zero, around 2×10^{-3}, or in terms of hole velocity $v_h \sim 0.75 v_T$, which is expected. Indeed, for out parameters $f'_{i,h} \sim 0$, this value provides a limit at which the effects of ion distribution over an electron-hole's dynamics become negligible.

D. Electric potential amplitude ϕ_0

As we saw in the previous parameter scans, the dynamics of electron-holes strongly depend on the value of the ion and electron equilibrium distributions. However, adjusting ϕ_0 changes the velocity-width of the hole. Therefore, an arbitrary electron-hole will experience different distribution gradients on the high-velocity side compared to the low-velocity side of the hole, including all the intermediate gradients in between. To accommodate for this effect due to the hole size $\Delta v_h \sim \sqrt{\phi_0}$, we introduce the effective electron equilibrium gradient, or effective gradient, $\partial_v f_{eq,eff}$ defined as the value of the electron gradient $f'_{e,h}$ weighted by the velocity-width of the electron-hole, in other words $\partial_v f_{eq,eff} \sim \partial_v f_{e,0} \sqrt{\phi_0}$.

Thus, we studied the effects of the electric potential amplitude on the electron-hole phasetrophy growth-rate. To do this, we performed nine simulations at fixed relative hole velocity $\delta v_h = 0.45 v_T$ and electron drift velocity $v_d = 1.00 v_T$. While varying the electric field amplitude in the interval $\phi_0\, e/T_e = [5 \times 10^{-3}, 1 \times 10^{-1}]$.

The growth-rate of the phasetrophy is plotted in Fig. 9 as a function of ϕ_0. First, we observe two regimes where the growth-rate increases as a power law of the potential amplitude: For $\phi_0 < 4 \times 10^{-2} T_e/e$, we measure $\gamma_h \sim \phi_0^{1.3}$, while for larger amplitudes, it increases as $\gamma_h \sim \phi_0^{0.8}$. Second, we observe a discrepancy between the

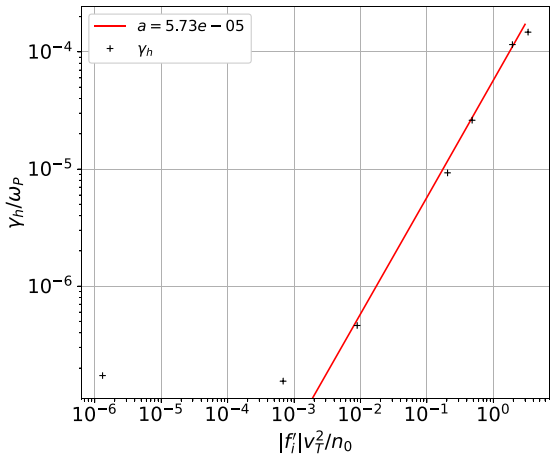

FIG. 8. Electron-hole phasetrophy growth-rate as a function of the absolute value of the ion equilibrium distribution gradient at the average hole velocity at the moment of the measurement. Growth-rate from numerical simulations in black crosses and linear data fitting in the high amplitude regime in the solid red line.

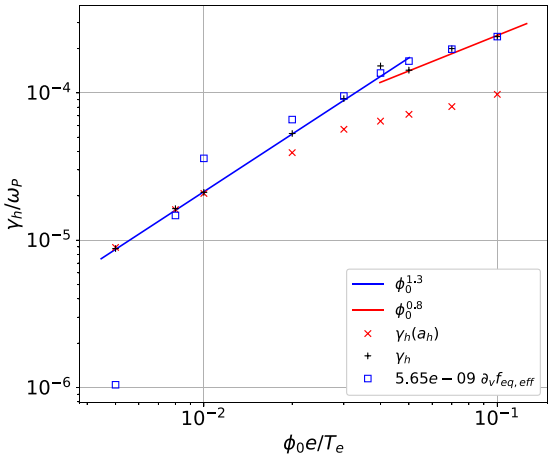

FIG. 9. Electron-hole phasetrophy growth-rate as a function of the initial amplitude of the electric potential. Growth-rate from numerical simulations in black crosses, $\gamma_h(a_h)$ is the growth-rate calculated from the acceleration, linear data fitting in the low and high amplitude regime in solid red and blue lines, and the effective electron equilibrium gradient normalized to the data in blue squares.

two measurements of the growth-rate γ_h from the phasetrophy and acceleration measurements for large values of ϕ_0. This can be explained by the fact that to obtain Eq. (14), we had to assume that the electron equilibrium distribution gradient remains constant in the velocity interval bounded by Δv_h, which is not the case for large values of ϕ_0. Nevertheless, for small values of ϕ_0, we observe agreement between both measurements. Finally, in Fig. 9, we show the effective gradient $\partial_v f_{eq,eff}$ normalized to the data. For large values of ϕ_0, we observe qualitative and quantitative agreement between the effective gradient and the growth-rate from numerical simulations. However, a large discrepancy is observed for the lower amplitude values. These results allow us to deduce that for small electron-holes, where the difference in gradient between the two extremums of the hole is small, then the value of the gradient is adequate to describe the electron-hole dynamics. On the other hand, for large electron-holes, the different regions of the electron-hole experience distinct gradients and, consequently, a distinct acceleration and growth of the phasetrophy. Thus, the velocity-width of the electron-hole must be taken into account. Note that the Schamel electron-holes limit our capacity to study this mechanism since the spatial and velocity widths are linked through Eq. (10), which expresses that the spatial-width is inversely proportional to the square root of the velocity-width. Therefore, by decreasing Δv_h, we increase Δx_h. However, this result is not physical since the ratio between phase-space structures remains narrow over a large ensemble of structures. This is the case for the electron-holes simulated in this manuscript.

V. CONCLUSION

In summary, we have investigated the phasetrophy growth and acceleration process of isolated electron-holes in phase-space. By means of four different parameter scans employing the Schamel electron-hole parameters, such as the relative electron-hole velocity δv_h, Schamel potential amplitude ϕ_0, the equilibrium ion gradient $f'_{i,h}$, and the equilibrium electron gradient $f'_{e,h}$, we have measured the phasetrophy growth-rate at distinct regimes and orders of magnitudes. First, we have shown that an isolated electron-hole grows as the simulation progresses, resulting in a change in its mean velocity, depth and phasetrophy. In particular, we have shown that an electron-hole is located in unstable regions of phase-space (i.e., located in between the ion and electron distribution maximas); it will experience a strong acceleration toward the electron distribution maxima. Second, we have quantified the effects of the ion and electron gradients on an electron-hole's dynamics. As the electron-hole approaches the ion distribution maxima, it will mainly experience a strong repulsion resulting in rapid acceleration and growth of phasetrophy, while further down the ion distribution, this effect decreases rapidly. Finally, we observed that the relative size of the electron-hole with respect to the size of the distribution functions has an essential effect on the hole's dynamics. In particular, we observed quantitative agreement between the effective gradient, which considers the size of the electron-hole and the different gradients it experiences at every point of its width, and the hole's phasetrophy growth-rate.

Therefore, we have measured and observed the effects of Schamel hole and plasma parameters, such as relative hole velocity δv_h, equilibrium gradients $f'_{i,h}$ and $f'_{e,h}$, and potential amplitude ϕ_0, on electron-hole dynamics in phase-space through numerical simulations. In particular, we have observed that the ion distribution function strongly influences electron-hole dynamics. Moreover, we have found that considering the different gradients of the distribution functions over the hole's width through the effective gradient can more accurately match the observed growth-rate for large electron-holes. However, further work is required to improve the understanding of electron-hole dynamics in phase-space. This study is subject to three caveats: first, increasing the mass ratio between ions and electrons to better understand real electron-holes.[53] Second, to analytically model the dynamics of an electron-hole whose shape is prescribed by Schamel's equations of an electron-hole. Moreover, to perform a larger set of simulations that will give us a more precise overview of electron-hole dynamics. Finally, to investigate the behavior of phasetrophy and acceleration during the interaction of two or more phase-space structures.[4,6,37]

ACKNOWLEDGMENTS

We acknowledge P. H. Diamond for his key role in developing the ideas presented in this paper.

This work was funded by the Agence Nationale de la Recherche for the Project GRANUL (No. ANR-19-CE30-0005). This work was granted access to the HPC resources of EXPLOR (Project No. 2017M4XXX0251), CINECA MARCONI under Project No. FUA36 GSNTITE, and NAISS DARDEL through Grant Agreement No. 2024-5701. This work has been carried out within the framework of the EUROfusion Consortium, funded by the European Union via the Euratom Research and Training Programme (Grant Agreement No. 101052200 – EUROfusion). Views and opinions expressed are, however, those of the author(s) only and do not necessarily reflect those of the European Union or the European Commission. Neither the European Union nor the European Commission can be held responsible for them.

AUTHOR DECLARATIONS

Conflict of Interest

The authors have no conflicts to disclose.

Author Contributions

A. Guillevic: Conceptualization (lead); Data curation (lead); Formal analysis (lead); Investigation (lead); Methodology (lead); Software (lead); Validation (lead); Visualization (lead); Writing – original draft (lead); Writing – review & editing (lead). **M. Lesur:** Conceptualization (equal); Funding acquisition (lead); Methodology (equal); Project administration (lead); Resources (lead); Software (equal); Supervision (lead); Writing – review & editing (equal). **D. Mandal:** Conceptualization (supporting); Methodology (supporting); Visualization (supporting); Writing – review & editing (supporting). **X. Garbet:** Writing – review & editing (supporting). **E. Gravier:** Writing – review & editing (supporting). **G. Lo-Cascio:** Writing – review & editing (supporting). **A. Ghizzo:** Writing – review & editing (supporting). **T. Reveille:** Writing – review & editing (supporting).

DATA AVAILABILITY

The data that support the findings of this study are available from the corresponding author upon reasonable request.

REFERENCES

[1]M. Lesur, P. H. Diamond, and Y. Kosuga, "Nonlinear current-driven ion-acoustic instability driven by phase-space structures," Plasma Phys. Controlled Fusion **56**, 075005 (2014).
[2]K. Saeki, P. Michelsen, H. L. Pécseli, and J. J. Rasmussen, "Formation and coalescence of electron solitary holes," Phys. Rev. Lett. **42**, 501–504 (1979).
[3]J. P. Lynov, P. Michelsen, H. L. Pécseli, J. J. Rasmussen, K. Saéki, and V. A. Turikov, "Observations of solitary structures in a magnetized, plasma loaded waveguide," Phys. Scr. **20**, 328–335 (1979).
[4]J. Lynov, P. Michelsen, H. Pécseli, and J. Rasmussen, "Interaction between electron holes in a strongly magnetized plasma," Phys. Lett. A **80**, 23–25 (1980).
[5]V. A. Turikov, "Electron phase space holes as localized BGK solutions," Phys. Scr. **30**, 73–77 (1984).
[6]A. Ghizzo, B. Izrar, and P. Bertrand, "BGK structures as quasi-particles," Phys. Lett. **120**, 191–195 (1987).
[7]H. L. Berk, B. Breizman, and N. Petviashvili, "Spontaneous hole-clump pair creation in weakly unstable plasmas," Phys. Lett. A **234**, 213–218 (1997).
[8]M. K. Lilley, B. N. Breizman, and S. E. Sharapov, "Effect of dynamical friction on nonlinear energetic particle modes," Phys. Plasmas **17**, 092305 (2010).
[9]H. L. Berk and B. N. Breizman, "Saturation of a single mode driven by an energetic injected beam. III. Alfvén wave problem," Phys. Fluids B: Plasma Phys. **2**, 2246–2252 (1990).
[10]T. H. Dupree, "Theory of resistivity in collisionless plasma," Phys. Rev. Lett. **25**, 789 (1970).
[11]H. L. Berk, B. Breizman, and M. Pekker, "Nonlinear dynamics of a driven mode near marginal stability," Phys. Rev. Lett. **76**, 1256 (1996).
[12]Y. Kosuga and P. H. Diamond, "On relaxation and transport in gyrokinetic drift wave turbulence with zonal flow," Phys. Plasmas **18**, 122305 (2011).
[13]R. J. Hamilton and V. Petrosian, "Stochastic acceleration of electrons. I—Effects of collisions in solar flares," Astrophys. J. **398**, 350 (1992).
[14]W. Liu, V. Petrosian, B. R. Dennis, and Y. W. Jiang, "Double coronal hard and soft x-ray source observed by RHESSI: Evidence for magnetic reconnection and particle acceleration in solar flares," Astrophys. J. **676**, 704–716 (2008).
[15]R. Boström, G. Gustafsson, B. Holback, G. Holmgren, H. Koskinen, and P. Kintner, "Characteristics of solitary waves and weak double layers in the magnetospheric plasma," Phys. Rev. Lett. **61**, 82–85 (1988).
[16]F. S. Mozer, R. Ergun, M. Temerin, C. Cattell, J. Dombeck, and J. Wygant, "New features of time domain electric-field structures in the auroral acceleration region," Phys. Rev. Lett. **79**, 1281–1284 (1997).
[17]S. R. Kamaletdinov, I. H. Hutchinson, I. Y. Vasko, A. V. Artemyev, A. Lotekar, and F. Mozer, "Spacecraft observations and theoretical understanding of slow electron holes," Phys. Rev. Lett. **127**, 165101 (2021).
[18]J. F. Drake, M. Swisdak, C. Cattell, M. A. Shay, B. N. Rogers, and A. Zeiler, "Formation of electron holes and particle energization during magnetic reconnection," Science **299**, 873–877 (2003).
[19]Y. V. Khotyaintsev, A. Vaivads, M. André, M. Fujimoto, A. Retinò, and C. J. Owen, "Observations of slow electron holes at a magnetic reconnection site," Phys. Rev. Lett. **105**, 1–4 (2010).
[20]B. Eliasson and P. Shukla, "Formation and dynamics of coherent structures involving phase-space vortices in plasmas," Phys. Rep. **422**, 225–290 (2006).
[21]P. H. Sakanaka, "Formation and interaction of ion-acoustic solitary waves in a collisionless warm plasma," Phys. Fluids **15**, 304–310 (1972).
[22]P. W. Terry, P. H. Diamond, and T. S. Hahm, "The structure and dynamics of electrostatic and magnetostatic drift holes," Phys. Fluids B: Plasma Phys. **2**, 2048–2063 (1990).
[23]W. Fox, M. Porkolab, J. Egedal, N. Katz, and A. Le, "Observations of electron phase-space holes driven during magnetic reconnection in a laboratory plasma," Phys. Plasmas **19**, 032118 (2012).
[24]R. C. Davidson, N. A. Krall, K. Papadopoulos, and R. Shanny, "Electron heating by Electron-Ion beam instability," Phys. Rev. Lett. **24**, 579 (1970).
[25]M. L. Bégué, A. Ghizzo, and P. Bertrand, "Two-dimensional vlasov simulation of raman scattering and plasma beatwave acceleration on parallel computers," J. Comput. Phys. **151**, 458–478 (1999).
[26]T. Boutros-Ghali and T. H. Dupree, "Theory of nonlinear ion-electron instability," Phys. Fluids **25**, 874–883 (1982).
[27]T. H. Dupree, "Theory of phase-space density holes," Phys. Fluids **25**, 277–289 (1982).
[28]T. H. Dupree, "Growth of phase-space density holes," Phys. Fluids **26**, 2460–2481 (1983).
[29]D. J. Tetreault, "Growth rate of the clump instability," Phys. Fluids **26**, 3247 (1983).
[30]R. H. Berman, D. J. Tetreault, T. H. Dupree, and T. Boutros-Ghali, "Computer simulation of nonlinear ion-electron instability," Phys. Rev. Lett. **48**, 1249–1252 (1982).
[31]R. H. Berman, D. J. Tetreault, and T. H. Dupree, "Simulation of phase space hole growth and the development of intermittent plasma turbulence," Phys. Fluids **28**, 155–176 (1985).
[32]S. M. Hosseini-Jenab and F. Spanier, "Study of trapping effect on ion-acoustic solitary waves based on a fully kinetic simulation approach," Phys. Plasmas **23**, 102306 (2016).
[33]C. Zhou and I. H. Hutchinson, "Plasma electron hole kinematics. II. Hole tracking particle-in-cell simulation," Phys. Plasmas **23**, 082102 (2016).
[34]S. M. Hosseini-Jenab and G. Brodin, "Head-on collision of nonlinear solitary solutions to Vlasov-Poisson equations," Phys. Plasmas **26**, 022303 (2019).
[35]D. Mandal, D. Sharma, and H. Schamel, "Ultra slow electron holes in collisionless plasmas: Stability at high ion temperature," Phys. Plasmas **27**, 022102 (2020).]
[36]H. Schamel, D. Mandal, and D. Sharma, "Evidence of a new class of cnoidal electron holes exhibiting intrinsic substructures, its impact on linear (and nonlinear) Vlasov theories and role in anomalous transport," Phys. Scr. **95**, 055601 (2020).
[37]A. Guillevic, "Nonlinear kinetic transport in high-temperature plasmas due to turbulence and vortices in phase-space," Ph.D. thesis (Université de Lorraine, 2023.).
[38]M. Lesur, Y. Idomura, and S. Tokuda, *Kinetic Simulations of Electrostatic Waves Using Cubic-Interpolated-Propagation Scheme* (Japan Atomic Energy Agency, 2006).
[39]M. Lesur, "The Berk-Breizman model as a paradigm for energetic particle-driven alfvén eigenmodes," arXiv:1101.5440 (2010).
[40]H. Schamel, "Stationary solutions of the electrostatic Vlasov equation," Plasma Phys. **13**, 491–505 (1971).
[41]M. M. Oppenheim, G. Vetoulis, D. L. Newman, and M. V. Goldman, "Evolution of electron phase-space holes in 3D," Geophys. Res. Lett. **28**, 1891–1894, https://doi.org/10.1029/2000GL012383 (2001).
[42]N. Carlevaro, G. Meng, G. Montani, F. Zonca, T. Hayward-Schneider, P. Lauber, Z. Lu, and X. Wang, "One dimensional reduced model for ITER relevant energetic particle transport," Plasma Phys. Controlled Fusion **64**, 035010 (2022).
[43]D. R. Durran, *Semi-Lagrangian Methods* (Springer, 1999), pp. 303–333.
[44]T. Nakamura, R. Tanaka, T. Yabe, and K. Takizawa, "Exactly conservative semi-Lagrangian scheme for multi-dimensional hyperbolic equations with directional splitting technique," J. Comput. Phys. **174**, 171–207 (2001).
[45]I. B. Bernstein, J. M. Greene, and M. D. Kruskal, "Exact nonlinear plasma oscillations," Phys. Rev. Lett. **108**, 546 (1957).
[46]K. V. Roberts and H. L. Berk, "Nonlinear evolution of a two-stream instability," Phys. Rev. Lett. **19**, 297 (1967).
[47]H. L. Berk, C. E. Nielsen, and K. V. Roberts, "Phase space hydrodynamics of equivalent nonlinear systems: Experimental and computational observations," Phys. Fluids **13**, 980–995 (1970).
[48]H. Schamel, "Non-linear electrostatic plasma waves," J. Plasma Phys. **7**, 1–12 (1972).
[49]A. Luque and H. Schamel, "Electrostatic trapping as a key to the dynamics of plasmas, fluids and other collective systems," Phys. Rep. **415**, 261–359 (2005).
[50]P. H. Diamond, S.-I. Itoh, and K. Itoh, *Modern Plasma Physics* (Cambridge University Press, 2010).
[51]P. H. Diamond, Y. Kosuga, and M. Lesur, "Dynamics of structures in configuration space and phase space: An introductory tutorial," in *Rotation and Momentum Transport in Magnetized Plasmas* (World Scientific, 2011), pp. 81–113.
[52]J. C. Mcwilliams, "The emergence of isolated coherent vortices in turbulent flow," J. Fluid Mech. **146**, 21–43 (1984).
[53]K. Saeki and H. Genma, "Electron-hole disruption due to ion motion and formation of coupled electron hole and ion-acoustic soliton in a plasma," Phys. Rev. Lett. **80**, 1224–1227 (1998).